Electronic Supplementary Information

Advancing Sustainable Practices in Li-ion Battery Cathode Material Recycling: Mechanochemical Optimisation for Magnetic Cobalt Recovery

Joshua Vauloup,[a] Cécile Bouilhac,[a] Nicolas Coppey,[c] Patrick Lacroix-Desmazes,[a] Bernard Fraisse,[a] Lorenzo Stievano,[a,b] Laure Monconduit,[a,b,*] Moulay Tahar Sougrati[a,b,*]

[a] ICGM, Univ Montpellier, CNRS, ENSCM, Montpellier, France

[b] RS2E, Réseau Français sur le Stockage Electrochimique de l'Energie, FR CNRS #3459, Amiens F-80039 Cedex 1, France

[c] SNAM, Viviez, France

SQUID magnetometery for metallic cobalt quantification

The accuracy of the metallic cobalt quantification by SQUID has been checked by weighing a precise amount of commercial Co(s) in by measuring the magnetic moment of the sample. The magnetic moment at saturation of the pure metallic cobalt adjusted by the sample mass should theoretically be 162 emu.g^{-1}. Experimentally, with the commercial Co(s), the magnetic moment at saturation is calculated at 166 ± 13 emu.g^{-1} (Figure S1, saturation estimated at 5 000 Oe). Therefore, quantification error will be ± 8 % of the results.

Figure S1 shows that cobalt (II and III) oxides (red dots) do not present a magnetic moment when exposed to a magnetic field meaning that its presence in the milled powder will not interfere with Co metal quantification.

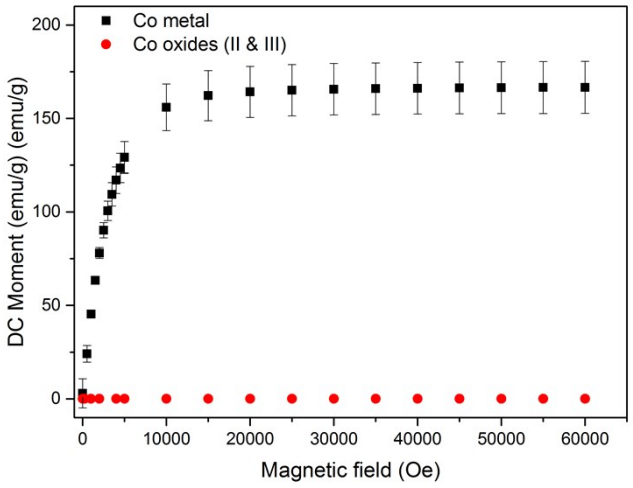

Figure S1 : Mass magnetic moment as function of the magnetic field applied. Analysis of commercial metallic cobalt and cobalt (II and III) oxide.

XRD fitting and phase determination

To determine the phases present in the milled powder, structural refinement was achieved with HighScore Plus® software using a pseudo Voigt profile function.

Figure S2 shows a diffractogram of a milled residue obtained using a Discover D8 XRD apparatus with a Cu source to avoid the $k_ß$ rays. Three main compounds are found for these milling conditions: $LiAlO_2$, metallic Co, and a partially reduced lithiated cobalt oxide: $Li_{0.185}Co_{0.815}O$.

Figure S5 to S6 represent XRD of a milled powder for different milling conditions. The main special feature for S3 is coming from Stainless Steel from the jare (related to the Figure 1 of the article). The presence of Iron and/or Iron Cobalt alloy is suspected. The Figure S4 is related to the Figure 3 of the article. This matching allows highlighting the Al_xCo_y alloy formation. The Figure S5 represent the diffractogram of a long milling experiment that has been exposed to additional amount of O_2 due to multiple sampling operation. This diffractogram aims to bring to light the only partial reduction of cobalt (Co(III) to Co(II)) with prominent peaks $Li_{0.185}Co_{0.815}O$ compound compared to metal cobalt. This diffractogram refers to discussion related to the Figure 7.b and c of the article. Finally, the Figure S6 allows showing the ZrO_2 pollution due to balls destruction due to large metal cobalt particles formation when a high amount of powder is used which leads to a high energy release (Cf. Figure 10 of the article). The Figure S6 also enable to highlight that without introducing further O_2 during the milling (without sampling before), no partially reduced cobalt in $Li_{0.185}Co_{0.815}O$ is observed.

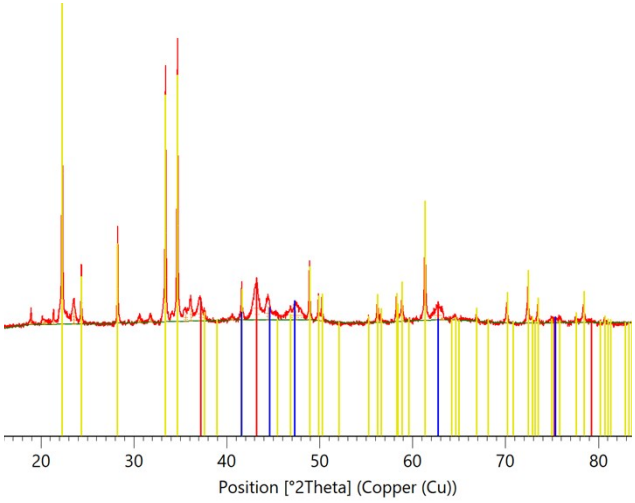

Compounds	$LiAlO_2$	Co	$Li_{0.185}Co_{0.815}O$
Crystal system	Tetragonal	Hexagonal	Cubic
Space group	P41212	P63/mmc	Fm-3m
Space group number	92	194	225
a (Å)	5.1687	2.5140	4.1850
b (Å)	5.1687	2.5140	4.1850
c (Å)	6.2679	4.1050	4.1850

Figure S2 : XRD of milled residue (red diffractogram) with milling conditions: 45 mL jare in ZrO_2, 2h , Al/LCO = 1, B/P = 0.14, 7 balls of 10 mm, 500 rpm, 15 min/10 min milling/rest cycle, under air.

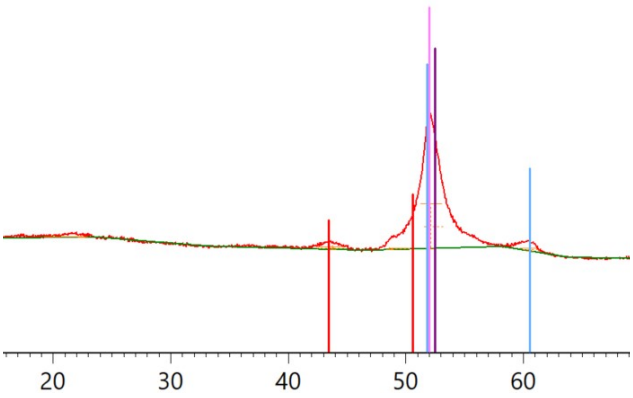

Compounds	Co_3Fe_7	Fe	Co	$Li_{0.185}Co_{0.815}O$
Crystal system	Cubic	Cubic	Cubic	Cubic
Space group	Pm3m	Im-3m	Fm-3m	Fm-3m
Space group number	221	229	225	225
a (Å)	2.8634	2.8860	3.5480	4.1850
b (Å)	2.8634	2.8860	3.5480	4.1850
c (Å)	2.8634	2.8860	3.5480	4.1850

Figure S3: XRD of milled residue (red curve)with (milled conditions: 45 mL jar in Stainless Steel, 14h , Al/LCO = 1, B/P = 0.14, 7 balls of 10 mm, 500 rpm, 15 min/10 min milling/rest cycle, under air.

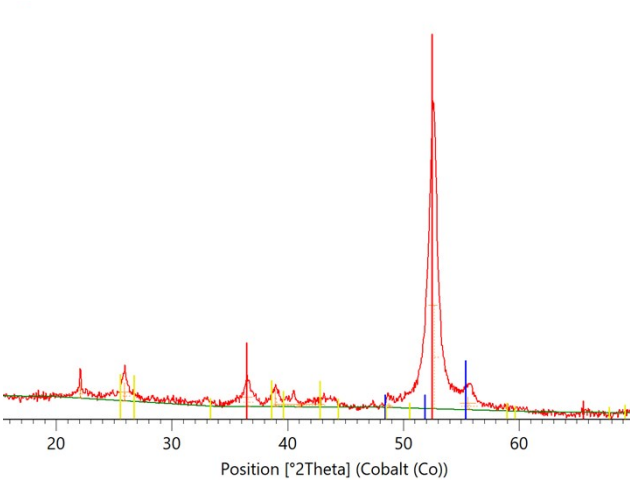

Compounds	$LiAlO_2$	Co	AlCo
Crystal system	Tetragonal	Hexagonal	Cubic
Space group	P41212	P63/mmc	Pm3m
Space group number	92	194	221
a (Å)	5.1687	2.5190	2.8620
b (Å)	5.1687	2.5190	2.8620
c (Å)	6.2679	4.0910	2.8620

Figure S4 : XRD of milled residue (red curve) with milling conditions: 45 mL jar in ZrO_2, 8h , Al/LCO = 1.5, B/P = 0.09, 4 balls of 10 mm, 500 rpm, 15 min/10 min milling/rest cycle, under air.

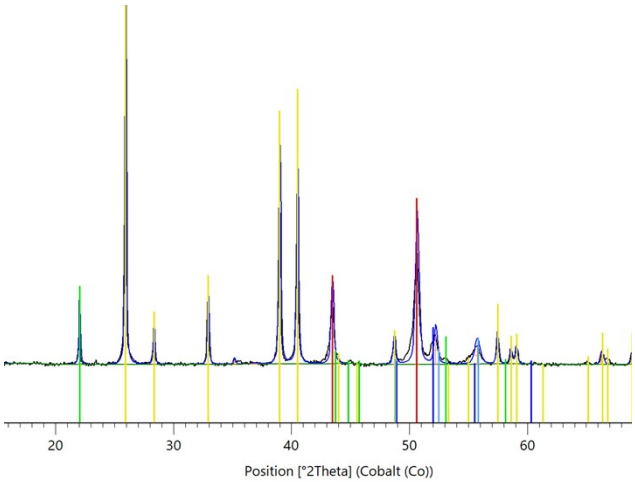

Compounds	$LiAlO_2$	Co		$Li_{0.185}Co_{0.815}$
Crystal system	Tetragonal	Hexagonal	Cubic	Cubic
Space group	P41212	P63/mmc	Fm-3m	Fm-3m
Space group number	92	194	225	225
a (Å)	5.1687	2.5031	3.5540	4.1850
b (Å)	5.1687	2.5031	3.5540	4.1850
c (Å)	6.2679	4.0605	3.5540	4.1850

Figure S5 : XRD of milled residue (blue curve) overlaid with milling conditions: 45 mL jar in ZrO2, 14h , Al/LCO = 1, B/P = 0.14, 7 balls of 10 mm, 450 rpm, 15 min/10 min milling/rest cycle, under air.

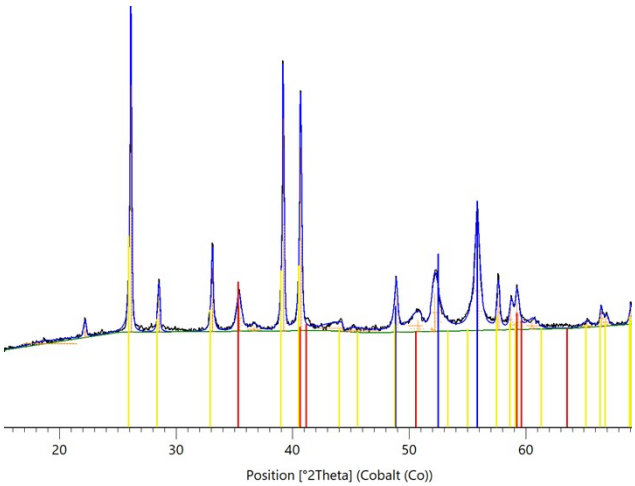

Compounds	$LiAlO_2$	Co	ZrO_2
Crystal system	Tetragonal	Hexagonal	Cubic
Space group	P41212	P63/mmc	P42/nmc
Space group number	92	194	137
a (Å)	5.1687	2.5031	3.5984
b (Å)	5.1687	2.5031	3.5984
c (Å)	6.2679	4.0605	5.1520

Figure S6 : XRD of milled residue (blue curve) with milling conditions: 45 mL jar in ZrO2, 3h , Al/LCO = 1, B/P = 0.24 (5 g of powder), 7 balls of 10 mm, 450 rpm, 60 min/10 min milling/rest cycle, under air.

Al-Co Phase diagram

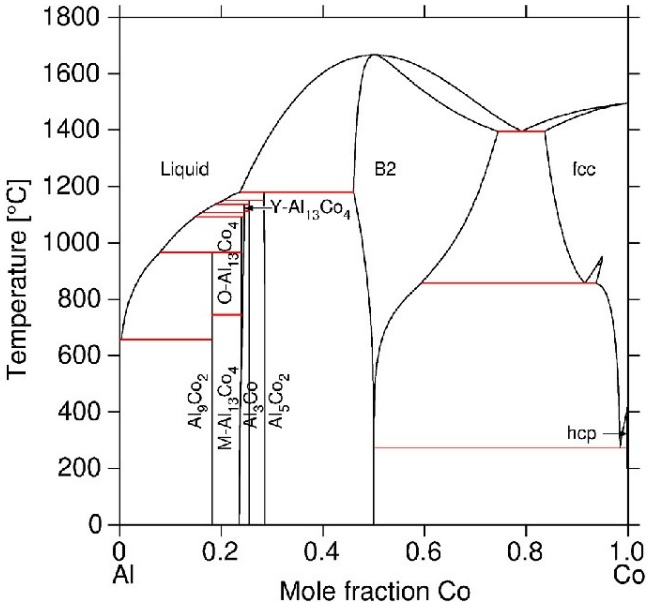

Figure S7 : Phase diagram of Al-Co

Reaction enthalpy calculation

Reaction ($\Delta H_{r,298K}$):

$LiCoO_2 + Al \rightarrow LiAlO_2 + Co$

$LiCoO_2$ formation enthalpy ($\Delta H_{f,LiCoO2,298K}$):

- From the oxides and oxygen at 298 K : -141 kJ.mol^{-1}[11]
  - ½ LiO + CoO + ¼ $O_{2(g)}$
- From the elements at 298 K: -678 kJ.mol^{-1}
  - Li + Co + $O_{2(g)}$

$LiAlO_2$ formation enthalpy ($\Delta H_{f,LiAlO2,298K}$):

- From the oxides and oxygen at 298 K: -12.880 kcal.mol^{-1}[12]
  - ½ LiO + ½ Al_2O_3
- From the elements at 298 K: -284.33 kcal.mol^{-1} = - 1 188.5 kJ.mol^{-1}
  - Li + Al + $O_{2(g)}$

With formation enthalpy of $LiAlO_2$ and $LiCoO_2$ from the elements:

$\Delta H_{r,298K} = \Delta H_{f,LiAlO2,298K} - \Delta H_{f,LiCoO2,298K}$ = -1 188.5 + 678 = - 510.5 kJ.mol^{-1} (1 cal = 4,180 J)

Powder/Balls mass ratio influence

Milled residue morphology difference as function of powder mass for a constant bead mass.

(a) (b)

Figure S8 : jars aspect after 2 h of milling under the following conditions: 500 rpm, 50 balls of 5 mm, Al/LCO = 1.0. a) 3 g of powder. b) 5 g of powder.

SEM-EDX analysis

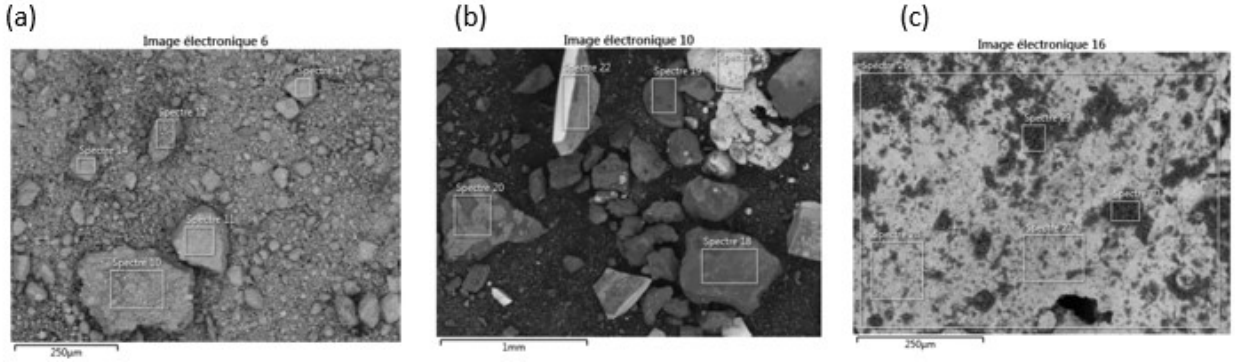

Figure S9 : SEM of residue after a milling of 2 h (a) and 3 h (b) and (c); (b) shows the powder residue and (c) the sheet like residue. EDX composition (at %) of the "spectrum XX" areas are listed in Table S1 (a),

Table S2 (b),

Table S3 (c).

Table S1 : Elemental composition from the "spectrum XX" area of different Figure S9 analysis.

Figure S9.a (at %)

Element	Spectrum 10	Spectrum 11	Spectrum 12	Spectrum 13	Spectrum 14
Co	26.7	17.7	26.4	29.6	23.7
Al	24.2	22.0	20.3	18.8	22.1
O	49.1	60.3	53.3	51.6	54.2
Tot	100	100	100	100	100

Table S2 : Elemental composition from the different areas of Figure S9b (at %).

Element	Spectrum 18	Spectrum 19	Spectrum 20	Spectrum 21	Spectrum 22
Co	5.8	7.1	16.6	5.4	3.0
Al	28.6	27.5	23.9	4.0	6.6
O	65.6	65.4	59.6	70.4	78.9
Zr	0.0	0.0	0.0	20.2	11.5
Tot	100	100	100	100	100

Table S3 : Elemental composition from the different areas of Figure S9c (at %).

Element	Spectrum 26	Spectrum 27	Spectrum 28	Spectrum 29	Spectrum 30
Co	57.6	67.2	66.5	25.3	23.4
Al	14.1	10.9	9.8	25.9	25.1
O	28.3	22.0	23.7	48.8	51.5
Tot	100	100	100	100	100

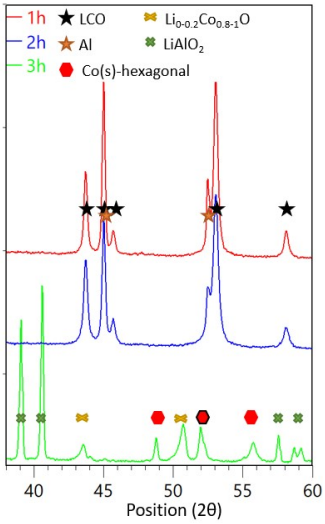

Figure S10 : XRD analysis of the milled residue related to the residues analyzed by SEM-EDX on Figure S9.

XRD analysis of the residue analyzed on Figure S9.a shows the presence of $LiCoO_2$ and Al, then that no reaction occurred (Figure S10), confirming the EDX analysis (Table S1), with the presence of Co and Al in equimolar proportion in the different areas of the milled residue.

After 3 h of milling, XRD shows a full structural change (Figure S10) with $LiAlO_2$, (Li)CoO and Co° apparition and the morphology of the powder changed with apparition of grey sheets. A heat increase of the jar is also observed. The grey sheet is supposed to be metallic cobalt due to its magnetic properties (tested with a magnet attraction). This is confirmed by SEM-EDX, which shows mainly Co° with presence of Al and O (

Table S3). Al can be assigned to powder entrapped on the surface of the particle (black spots) and O to surface oxidation. Some white large particles attributed to ZrO_2 are also present, coming from balls damage.

Table S2 gives the elemental composition of different areas of this milled powder residue. The other parts are mainly composed of Al and O with traces of Co. This observation supports that the sheet like particles are metallic Co and the remaining powder consists of $LiAlO_2$.

Lattice parameters evolution of the reagents (Al and LCO) as function of milling time

Method: Rietveld refinement (FullProf® software).

Observations: No significant changes for the a (= b) lattice parameter of LCO during the milling, while c parameter progressively decreases until 7 h of milling. This decrease can be attributed to LCO inter-lamellar distance reduction due to a delithiation. Regarding aluminum, the lattice parameters mainly decrease in the first moment of the milling. A longer milling does not affect the Al crystallographic parameters.

Controlled atmosphere

All the experiments were carried under air atmosphere. To study the influence of the oxygen on the cobalt reduction, some experiments were also performed under argon. The jars were filled and opened in a glove box under argon. Only a very slight difference in terms of the LCO conversion to Co metal as a function of milling time is observed (Figure S12). The oxygen-free atmosphere does not influence the reduction of LCO. However, the oxygen influence is likely limited in these experiments where the high-energy ball milling leads to a fast reduction. To highlight the influence of oxygen, experiments with a lower milling energy should be carried out or a temperature measurement has to be performed to determine more accurately the reaction triggering.

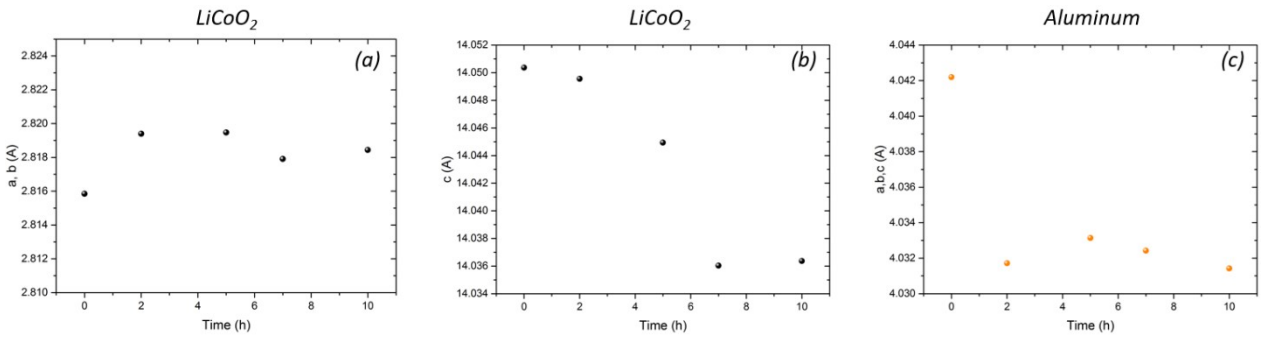

Figure S11: Lattice parameters evolution as function of milling time for (a) a (= b) of $LiCoO_2$, (b) c of $LiCoO_2$ and (c) a (= b = c) of aluminum.

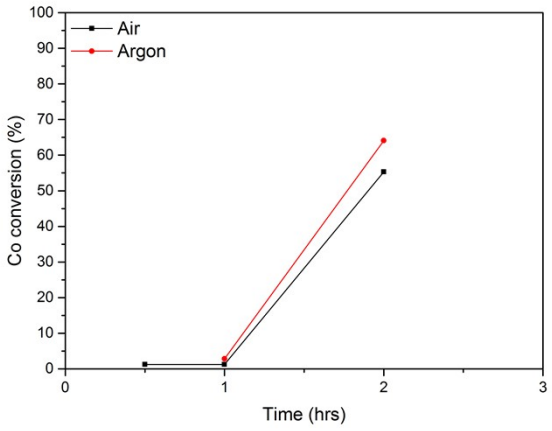

Figure S12 : Co conversion rate as a function of milling time under air (black) and under argon (red). Milling conditions: 500 rpm, 3 g of powder (Al + LCO), Milling/rest cycle = 15 min/ 10 min, Al/Co = 1.0, P/B = 0.15, 50 balls of 5 mm.

1 M. Wang and A. Navrotsky, *Solid State Ionics*, 2004, 166, 167–173.

2 J. P. Coughlin, *J. Am. Chem. Soc.*, 1957, **79**, 2397–2399.